EUROPEAN ORGANIZATION FOR NUCLEAR RESEARCH
CERN - SPS DIVISION

CERN LIBRARIES, GENEVA

CM-P00052099

CERN-SPS/ABT/77-16

A LAMINATED-IRON FAST-PULSED MAGNET

P.E. Faugeras, C.G. Harrison, M. Mayer, G.H. Schröder

Geneva, August 1977

CGH/jf

CONTENTS

		Page
1.	Introduction	1
2.	Yoke and Conductor Design	2
3.	Eddy Current Effects	6
4.	Mechanical Design	7
5.	Construction	8
6.	Pulse Generator and Transmission Line	10
7.	Performances	11
8.	Conclusions	12
Acknowledgements		12
References		13
Appendix :	Eddy Current Effects in Pulsed Fields	15
Figures 1 - 20		

1. Introduction

In the SPS Beam Dumping System [1], two pairs of fast pulsed magnets deflect the circulating beam vertically and horizontally from its normal closed orbit, and onto a large absorber block. Two MKDV kickers produce a quasi-rectangular field pulse of 23 μs duration (this being the SPS revolution period) causing a vertical deflection of 44 mm at the absorber block, while two MKDH sweepers give a horizontal deflection ramping during 23 μs to a peak of 25 mm. On the 'flat top' of the MKDV pulse, oscillations of ± 10 % of the primary deflection are introduced. The proton beam is thus dumped into the absorber block during one revolution. Dumping may occur at any energy, but the dumping of a 400 GeV/c pencil beam of 10^{13} proton would produce thermal shock waves which would ultimately deform any solid absorber. The sweeper's 25 mm horizontal deflection and the kicker's 10 % oscillations were introduced to sweep the dumped beam over an area of about 200 mm^2 giving a reduction of one to two orders of magnitude in the peak stress induced in the absorber block (see Fig. 1).

This report concerns the design and construction of the MKDH sweeper magnets, their pulse generators and pulse transmission lines. The sweepers are unusual in being relatively fast pulsed magnets constructed from iron laminations without the use of organic materials and operating entirely in vacuo.

The MKDH magnets are required to produce a deflection of 1.18 mrad, which implies a kick strength of 1.58 T.m at 400 GeV/c. Since the pulse shape is a ramp, rather than a rectangle, the main Fourier component is at about 10 kHz, rather than 10 MHz. In view of this limited frequency range it was decided to try to build the magnet yoke with thin laminations of transformer steel, rather than the ferrite blocks used for the other SPS kickers. The resulting gain in saturation field gives a 2-3 fold reduction in length. Since the sweepers were to be installed downstream of the kickers, the reduction in length leads also to a small reduction in the required vertical aperture, due to the reduced 'lever-arm' of the kicker vertical deflection. Other advantages of iron are its ready availability and greater resistance to mechanical damage, e.g. during

construction or installation. Disadvantages are the need to insulate the 'hot' conductors, the difficulties of accurately stamping, assembling and supporting several thousand thin laminations, eddy current problems and a higher remanence. A consequence of the move to a higher field is an increase in peak current to 30 kA compared to about 10 kA for a ferrite magnet. The use of a small, low inductance magnet also emphasises the need to avoid stray inductances. Further design criteria were that no organic materials be used and the entire yoke be under vacuum at less than 10^{-7} Torr.

The magnet was required to produce a good-field region of 90 x 56 mm in the transverse plane with less than 2 % peak non-uniformity. It was also required for this magnet that the peak voltage to ground should not exceed 4 kV. These conditions lead to a choice of two separate magnets each with a physical length of 1200 mm and a peak field of 0.65 T produced by a single-turn coil. The pulse generator was chosen to be a conventional capacitor discharge using ignitron switches to give a sinusoidal rise and an exponential fall. The sinusoid was to be used up to a phase of 75^{o} so the peak-field was 0.67 T after 24 μs. Figure 2 shows the main system parameters.

2. Yoke and Conductor Design

The yoke was designed by studying the calculated field distribution in the gap given by the FORTRAN program MAGNET [2]. MAGNET treats two-dimensional d.c. fields and pulsed conditions were simulated by using sheet current distributions in the conductors and also by modifying the $\mu_r(B)$ curve (see below). The current was assumed to be confined by eddy current effects in the conductors to the skin depth, which is 0.5 mm in copper at 10 kHz. Since the magnet's impedance is almost purely inductive, it was further assumed that the sheet currents would choose the path of minimum inductance, i.e. a single sheet on the inner face of the inner

3. Eddy Current Effects

During the current pulse the changing excitation field, $\underline{H}$, induces sheet currents in the surfaces of the laminations. These currents, flowing roughly in the skin depth, δ, oppose the excitation and impede the penetration of the field into the lamination. The flux distribution through the lamination thus has the profile shown in Fig. 11. This effect can be summarised by saying that in the changing excitation field $\underline{H}(\omega)$, the lamination carries an average flux density of roughly $\frac{\delta}{a} \cdot \mu_r \mu_o \underline{H}(\omega)$, where δ is defined in the Appendix and a is half the lamination thickness, μ_r is the relative permeability and ω is the frequency of the pulse. Now in the magnet the circulating flux is determined essentially by the ratio of pulse current to gap height. Thus to reach the same average induction the surface layers must reach higher inductions, this is achieved by a greater drop of excitation (magneto motive force, mmf) in the yoke, typically a few per cent. There are two points to note here :

(i) if the ratio $\frac{\delta}{a}$ is small, the surface layers may approach saturation for quite small average inductions,

(ii) this highly non-linear system can be described phenomenologically by an effective permeability $\mu_{eff} = \mu_{eff}(\delta, a, \mu_r)$, where of course $\delta = \delta(\mu_r, \omega)$ (see Appendix). μ_{eff} is always less than μ_r, sometimes dramatically so for high permeability materials.

Using a table of μ_{eff} v. B in the program MAGNET enables the effects of eddy currents on the gap field uniformity and on the loss of mmf to be calculated. Using normal silicon electrosteel with thickness in the range 0.125 mm to 0.5 mm (δ is typically 0.14 mm), no significant changes in the non-uniformity due to eddy current effects could be found by calculation and as seen in Fig. 9, no significant perturbation could be measured on the prototype magnet.

retaining clamps must be applied and these might cause wearing of the insulation. A composite insulation was applied in which the conductor was first enveloped in two 0.125 mm Kapton H foils *) and these were protected by two sheaths of woven glass-fibre of average thickness 0.325 mm (Fig. 5). The Kapton foil was the only organic material in the magnet and has a radiation resistance greater than 10^{10} Rads. Consideration of the relative permittivities of the two types of insulation shows that normally the glass-fibre sheaths support most of the electrical stress, but the Kapton foils are necessary to prevent arcing through or along the glass-fibre. D.c. tests showed that this insulation would fail at about 16 kV by surface flash-over from the central terminals, along the glass-fibre to the yoke. It was not possible to produce a breakdown through the Kapton to the yoke. The ionisation inception level was about 12 kV.

In each half-magnet 26 clamp springs pressed well-rounded pads against the hot conductor's glass-fibre insulation (see Fig. 5). The springs were recessed in the gap in 2 mm long openings left by enlarging the apertures of packets of 6 laminations. (Previous experience had shown that such recesses have no significant effect on the field [5].) The spring constant was 490 N/mm.

At the ends of the magnet the hot and cold conductors were connected by copper loops encircling the aperture. At the centre of the magnet the two hot terminals were insulated by Vetronite blocks and clamped against the ends of the two half-magnets. The cold conductor in the central region was brought across the gap by a copper loop on each half-magnet the two loops being joined above and below the hot terminals. This was to avoid inductance in the cold conductor which could have led to earth loops through the magnet's vacuum tank. See Fig. 10.

---

*) Du Pont de Nemours, Geneva, Switzerland.

the oxide layer of the laminations.) An air-gap of 0.15 mm was allowed between the cold conductor and the yoke, which also allowed for possible deviations from straightness in the yoke. To provide vertical and horizontal location, the cold conductor was made taller than the gap and fitted into an enlarged channel in the laminations. This removed some of the current sheet from the gap and produced a strong non-uniformity. The inner face of the cold conductor was extended 1 mm into the gap and a sheet current flowing on that face and on the outer face (there being no inductance to minimise in the cold conductor) gave an acceptable calculated uniformity (see Fig. 4). The cold conductor was welded to the front plate (see below) to give support and good thermal contact.

The overall calculated non-uniformity of the gap field on the centre-line, showed a rise near the hot conductor and a droop near the cold conductor (characteristic quadrupole error). These errors can be compensated by installing the two sweeper magnets facing in opposite radial sense. The net non-uniformity was then as shown in Fig. 8.

The real gap-field of the prototype was studied using long pick-up coils, while pulsing the magnet in air. The field distribution was measured with a spatial resolution of 5 mm and a relative accuracy better than 0.2 %. The results are plotted on Fig. 9, and show the real field to be rather better than the predictions. The remanent field after a 30 kA pulse was about 2 G on the centre line. (This remanent field in the two magnets causes a perturbation of the SPS closed orbit. At injection with a 10 GeV/c beam, the resulting betatron amplitude is 0.5 mm.)

The hot conductor insulation was required to withstand a peak of 4 kV at the central terminals. However, the main considerations for the insulation material were high radiation resistance and high mechanical strength and resistance to abrasion. The peak acceleration expected for the hot conductor was 4.10^3 m.s^{-2} so that strong

conductor and on both faces of the outer conductor. The non-uniformity of the kick produced by the end-fields was neglected. Reference 3 shows that the end-field effectively extends the magnetic length by half the gap height at each end for a d.c. magnet. This amounts to about 9 % in this case so that very large non-uniformities here would still be acceptable. In a pulsed magnet, however, the eddy currents in the end-plates (see Fig. 10) strongly restrict the extent of the end-fields.

A C-shaped yoke was chosen for ease of construction and because only the inner conductor need be insulated. (The outer conductor acts as a current septum and has virtually no inductance.) The insulation requirement of the inner, 'hot' conductor was halved by splitting the magnet into two half-magnets and feeding the current from the two centre terminals (see Fig. 3).

Space was left around the 'hot' conductor for 1 mm of insulation (see below). This air-gap considerably impairs the calculated field uniformity at the inside of the aperture: several per cent lower in the corners and a few per cent higher on the centre line over a width of about 10 mm [3]. Although methods exist for the improvement of this type of field distortion, in practice they were excluded here by the chosen method of construction. The required good-field region was therefore produced by making the gap 10 mm wider than the specified aperture, the 10 mm non-uniform area being excluded from the aperture (see Fig. 4). This area would in any case have been excluded, since it is partially occupied by the spring clamps required to restrain the 'hot' conductor (see Fig. 5). The calculated uniformity is further impaired by the sheet current distribution as compared to a uniform distribution (see Fig. 6). Rounding the corners of the 'hot' conductor to a 2 mm radius to reduce electrical stress and ease assembly has only a slight effect however (see Fig. 7).

At the outer, 'cold' conductor a thin insulation layer was foreseen to prevent short-circuiting the laminations, which could worsen eddy current problems. (Finally this was omitted, reliance being placed on

The lamination thickness was therefore defined by requiring that the surface induction should not approach saturation. This avoided too much hysteris heating and suggested a thickness below 0.5 mm. Very thin laminations were avoided since they posed special difficulties of rolling, stamping and assembly and a thickness of 0.35 mm was chosen. At this thickness the yoke mmf drop would be about 1 % but it was not measurable on the prototype magnet. This thickness requires about 3400 laminations for each magnet.

To avoid eddy currents circulating around a number of laminations, the laminations must be insulated from one another. In view of the high radiation levels in the SPS and the high vacuum in which the magnets have to work, the classical techniques of varnish or epoxy resins were avoided and the insulation was produced by oxidizing the laminations. Consideration of the emf induced around a loop embracing two laminations showed that for the loop current to be small compared to the current induced in a single lamination, a surface resistivity greater than 0.005 ohm.cm^2 was required. After oxidization by heating in air at 380° C for two hours followed by a slow cool, a surface resistivity of typically 0.04 ohm.cm^2 was achieved.

4. Mechanical Design

Eddy current heating effects in the non-magnetic parts - tie-bars, end-plates, springs, etc. were estimated from calculated values of the fields in their neighbourhood. These, together with resistive heating in the conductors and eddy current and hysteris heating of the yoke, yielded on estimated total dissipation of 80 J/pulse. The thermal impedance between the hot conductor and the external environment was estimated to be sufficiently low as to give peak temperatures of 40° C (30° C after connecting a 3 mm copper plate between the cold conductor and the tank base, see Fig. 5). However, the impedance was too high to give a reasonable cool down time after baking the magnet to improve the vacuum. It was therefore decided to cool the front or open face of the yoke and the cold conductor by passing water through channels in the front plate. Using this cooling, it was possible to cool the magnet from 140° C to room temperature in 3-4 hours.

The yoke was designed to be made of no more than the 3400 laminations and two end-plates clamped together by four tie-bars. This assembly was to be sufficiently rigid, the rigidity deriving mainly from the tension in the tie-bars, for it to be self-supporting; its 400 kg weight was to rest only on feet on the outer end-plates. A further contribution to the rigidity of the final magnet came from the front-plates which were strongly dove-tailed to the yoke (see Figs. 5 and 14).

The vacuum characteristics of 3400 tightly compressed laminations, representing about 200 m^2 of oxidized surface were unknown. Air was certainly trapped between laminations and previous magnets of this type had either used many fewer laminations [4] or had potted the entire yoke in epoxy [5]. To assist the out-gassing of the yoke, a heater was installed on top of the yoke enabling a bake-out at up to 120° C. The vacuum tank was normally pumped by two sputter ion pumps having a combined capacity of 800 ℓ/s at 10^{-6} Torr. A turbo-molecular pump backed by a large two-stage rotary pump was used for roughing out.

Figure 13 shows the pump-down curve for the new prototype magnet. Subsequent pump-down in the SPS tunnel required only 4 days to reach 10^{-7} Torr without repeating the bake-out. A surprise on first pulsing the magnet was the sympathetic pulsing of the pressure, initially up to 10^{-5} Torr, as further air was expelled from the yoke. After several hours of pulsing, these pressure pulses died away and the stable operating pressure was $7 - 14.10^{-9}$ Torr, essentially identical to the ferrite kickers.

5. Construction

Silicon electro-steel was readily obtained *) in rolls 300 mm wide and 0.35 mm thick. The surfaces were neither phosphated nor oiled. The laminations were stamped to a high accuracy **) with a maximum

---

*) Cockerill-Ougré, Liège, Belgium.

**) SIFOP, Besançon, France.

burr of 0.09 mm. They were subsequently suspended on racks at 1 mm intervals, cleaned by vapour degreasing and then oxidized (see above), in a furnace of the CERN Central Workshops. The laminations were again cleaned by vapour degreasing to remove any dust or loose oxide and then baked at 120°C in a vacuum oven to remove traces of degreasing fluid. The racks were sealed in plastic sheeting and flushed with dry nitrogen.

The assembly 'jig' was a girder onto which the laminations could be stacked with the gap opening downwards. Lateral guidance was provided by two brass bars bolted to the girder. The first step was to mount the central end-plate section rigidly on the girder and then to stack laminations on either side using the tie-bars as guides. Alternate packets of 140 laminations were inverted to compensate for rolling errors in the sheet steel. Between the packets six laminations with enlarged apertures were inserted to provide the spring recesses. After stacking the end-plates were added and the tie-bars progressively tightened until the yoke ceased to contract as air was expelled. This lasted a few days. The bars were tightened to about 2/3 of their nominal tension (3 tons) and then the yoke was lifted off the 'jig' and placed upright on a marble top. Fine adjustments were made to the straightness by varying the tie-bar tensions, giving a final straightness better than 0.3 mm in both planes over the 1200 mm yoke. The packing factor was 99 %.

The Kapton H insulation was formed onto the conductors by wrapping and baking overnight at 140°C. The woven glass-fibre sheaths were drawn over the conductors and clamped at the ends. The clamps were electrically connected to the conductors. The insulated conductors were then inserted sideways into the gap and the clamp springs positioned in the recesses. The front-plate bearing the cold conductor and water feedthroughs was firmly bolted on and the retaining bolts wined together (see Fig. 14). About two weeks were required to reach this stage. After completing the conductor connections the magnet was positioned on the vacuum tank base.

6. Pulse Generator and Transmission Line

The decision to split the magnet in two halves and bring out two live terminals (see Fig. 3) had important consequences for the pulse generator and transmission line, though these were otherwise relatively conventional.

The magnet had an inductance of 2.4 μH and it was required that the transmission line - having a length of about 150 m - should not add more than 2.0 μH. This would normally imply the installation of 12-20 triaxial pulse cables, but one manufacturer*) had the idea of binding four standard coaxial pulse cables (7.0 L/10.4) together surrounding them with a common ground screen. A special connector was developed which enabled these four cables to be connected in parallel to a low-inductance socket (see Fig. 15). Four such four-fold cables were installed for each magnet giving an inductance of about 1.2 μH. A special insulating layer was placed around the four single cables, since the coaxial shield was also pulsed up to 4 kV, and the ground shield around this (see Fig. 15). To equalise the capacitance to ground of the positive and negative conductors, two of the four fold cables had their polarities reversed at each end; this equalisation should avoid 'ringing' on the pulse due to parasitic resonances.

The pulse generator was essentially a 70 μF capacitor bank discharged into the combined inductance of the magnet and the transmission line. To avoid excessive inverse voltage on the capacitors, the negative swing after the crest of the sinusoid was clamped by a crowbar ignitron in series with a low-inductance resistor (0.14 ohm). This circuit (see Fig. 16) give a calculated peak inverse voltage of about 24 %. Over 90 % of the pulse energy was returned to the resistor. Note that the power supply **) was single-ended whereas both terminals of the capacitor bank were 'live'. The charging current therefore

---

*) Felten & Guillaume Kabelwerke AG, Köln, W. Germany.
**) 15 kV/1A by Philips of Eindhoven, Netherlands.

flows along an earth path to the magnet and back along the negative conductors of the cables. The capacitor bank was constructed of fifteen 4.65 μF/12 kV units *) their terminals being joined by a stripline. The switches were BK 178 ignitrons **). See Fig. 17.

The pulse generator and cables were tested by pulsing at 10 kV for over 1 million pulses without failure.

7. Performance

As has been shown above the performance of the sweeper magnet in terms of vacuum and magnetic field production was entirely satisfactory. After a life test of 1 million pulses to the peak field at a repetition period of 4 s, the vacuum tank of the prototype magnet was opened and a search made for signs of wear: none was found. The two final magnets were constructed with only minor design changes - chiefly to the fabrication of the front cooling plate - and after testing they were installed in LSS4 of the SPS ring, see Fig. 18. The prototype was also upgraded to the final design to serve as a reserve magnet. No failures were found in these magnets during the first year of SPS operation.

Figure 19 shows an interesting eddy current effect worthy of further study. The two traces are the magnet current and magnet field observed during prototype tests. The magnet current shows rather strong ripples at the start of the rise: these are due to voltage wave reflections along the cable. Note that they are greatly attenuated in the field pulse. The interest lies however in the different rise times. As was noted above, the effect of eddy currents in the yoke is to delay the rise of the induction and this is clearly seen here. What is gratifying to see, however, is that in the case of an LC discharge it is the current pulse which is distorted and the field pulse remains almost ideal. Why is this ?

---

*) Passoni & Villa, Milano, Italy.
**) English Electric Valve Co., Chelmsford, England.

Basically the answer lies in the behaviour of the electrical circuit :

$$V = \dot{\Phi}$$

where $\dot{\Phi}$ is the rate of change of flux through the single-turn coil.

Thus the real gap flux appears quite strongly in the electrical response. Of course the flux-current relationship is distorted by the eddy current effects, drawing a larger current from the capacitor and thus discharging it more rapidly, but the pulse shape is very much less distorted than might have been expected.

8. Conclusions

It is thus possible to produce compact, powerful fast pulsed magnets with a response up to at least 10 kHz by using a laminated, oxide insulated iron yoke. The mechanical problems associated with the use of thin laminations can be overcome and eddy current effects avoided. The vacuum performance of such a magnet can be quite comparable to that of ferrite magnets.

The SPS beam dump system as a whole is being reviewed for possible operation at higher beam intensities and energies; MAGNET calculations have shown that the field uniformity of the MKDH does not degrade appreciably on going up to 500 GeV/c and tests on the prototype showed it to withstand the additional electrical and mechanical stress.

Acknowledgements

We wish to thank the suppliers and members of the CERN personnel who assisted the design and construction of the MKDH magnets, especially R. Chappuis and P. Gerdil of the SPS Division.

References

1) P.E. Faugeras, C.G. Harrison, G. Schröder, Design Study of the SPS Beam Dumping System, Lab II/BT/Int./73-5.

2) Program MAGNET : Two-dimensional Magnetic Fields including Saturation (7600 Program Library T600).

3) R.L. Keizer, Calculation of DC Operated Septum Magnets - Magnetic Field Calculations, CERN/SI/Int.MAE/71-2.

4) J. Dupin, E. Hazledine, A.J.T. Holmes and A. Knezovic, Measurements of a 2 x 500 mm Septum Magnet, Lab II/BT/Int.Note/73-6.

5) H. van Breugel, R. Cuénot, S. Hérin and B. Kuiper, The Septum Magnets for the Fast Ejection System of the Serphukhov 70 GeV Proton Accelerator, PS/FES/72-4.

6) D. Reistad, Simple Expressions to Evaluate Eddy Current Effects in Laminated Magnets, ISR-BT/68-42.

7) P.E. Faugeras, E. Frick, C.G. Harrison, H. Kuhn, V. Rödel, G. Schröder and J.P. Zanasco, The SPS Pulsed Magnet Systems, CERN/SPS/BT/76-1.

8) F. Schäff, Analytic Expressions for Eddy Current Field Components in Quasi-Rectangular Bending Magnet Vacuum Chambers, CERN/SI/Note MAE/71-4.

APPENDIX

Eddy Current Effects in Pulsed Fields

A lamination of thickness 2a lies in the x-y plane and is subject to an external magnetic field H_o directed along y. If the field is only slowly varying with time, the whole lamination is magnetised to an induction

$$B_o = \mu_r \mu_o H_o \qquad (1)$$

where μ_r is the relative permeability of the iron at this induction.

If the field is now pulsed, with a pulse shape having a characteristic Fourier component ω and a repetition frequency very much less than ω, eddy currents are induced during the rise of the pulse which hinder the field penetration. If we take μ_r = constant, an analytic solution of Maxwell's equations gives :

$$B_y(Z) = Bo \frac{\cosh (I+j)z/\delta}{\cosh (I+j)a/\delta} \qquad (2)$$

Here B_o is the surface induction, i.e. at $z = \pm a$ and δ is the skin depth :

$$\delta = \sqrt{\frac{2}{\mu_r \mu_o \omega \sigma}} \qquad (3)$$

where σ is the conductivity of the iron.
The average flux carried by the lamination is thus :

$$B_m = \frac{1}{2a} \int_{-a}^{a} |B_y(Z)| dz \qquad (4)$$

$$= Bo \cdot const = \mu_o H_o const$$

We may call this last constant an effective relative permeability μ_{eff} since it relates the average flux carried by the lamination to the field H_o.

$$\mu_{eff} = \frac{Bm}{\mu_o H_o}$$

$$= \mu_r \frac{Bm}{Bo} \quad \text{after substituting (i)}$$

Since in reality μ_r is not constant, equation (2) should not be integrated directly. However, the surface induction $B_o(H_o)$ is known and we can numerically integrate through the lamination, re-evaluating $\mu_r\left(B_y(Z)\right)$ at each point :

$$B_i = B_{i-1} + \Delta z \cdot \left|\frac{\Delta B_{i-1}}{\Delta z}\right|$$

where $$\frac{\Delta B_{i-1}}{\Delta z} = \frac{dBz}{dx} = -\frac{1}{\delta_{i-1}} \cdot \frac{\sinh x/\delta_{i-1}}{\cosh a/\delta_{i-1}}$$

where δ_{i-1} is equ. (3) evaluated at the point i-1.
We take $\Delta z << \delta_{i-1}$. In this way the function By(z) may be evaluated for various values of B_o . B_m may be obtained by integrating By(z) and hence $\mu_{eff}(B_m)$. In practice there is little error in taking μ_r = const. and evaluating equ. (2) directly. Figure 20 shows the $\mu_{eff}(B_m)$relations for a lamination thickness of 0.3 mm of silicon at $\omega = 2\pi$ 9.05 kHz.

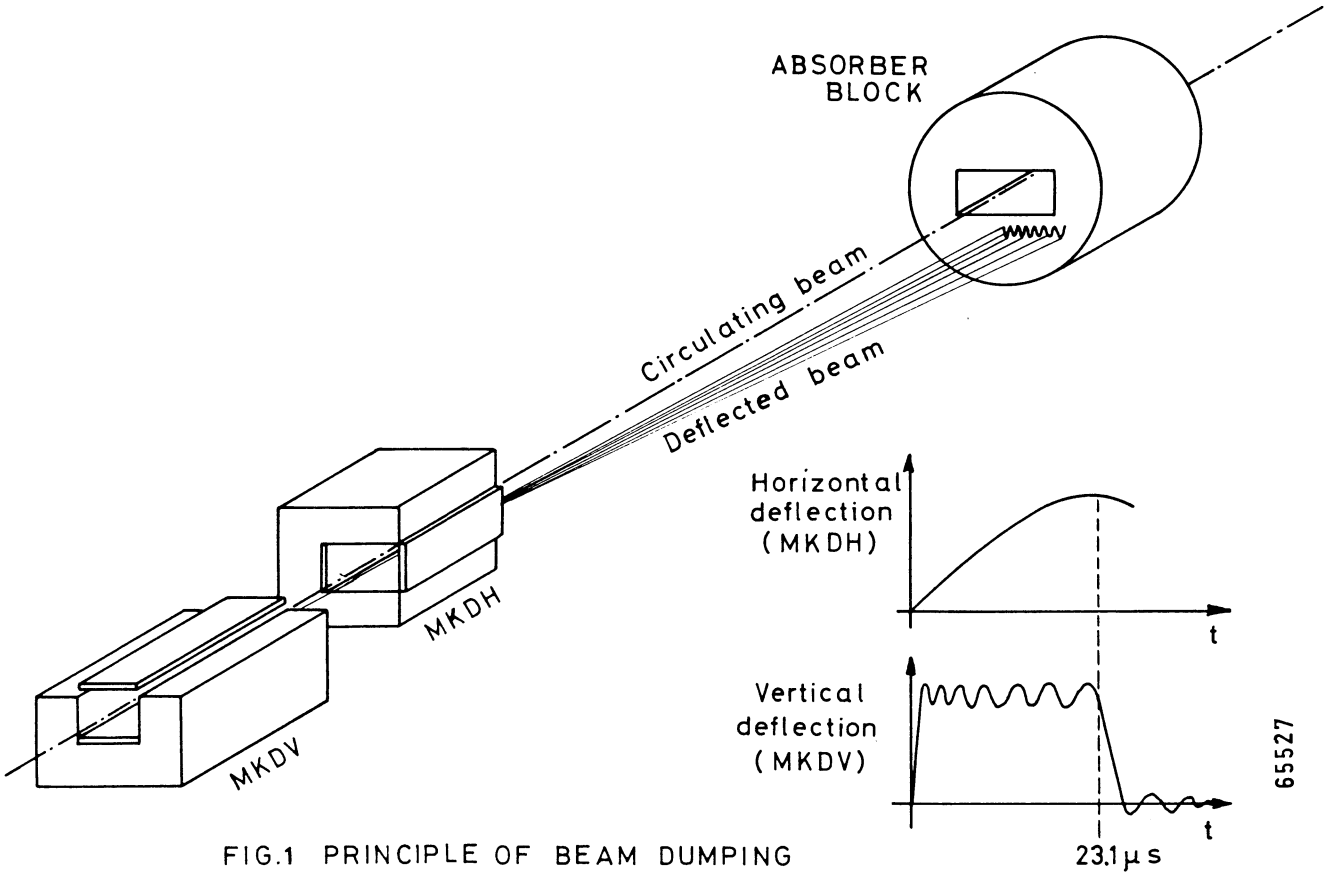

FIG.1 PRINCIPLE OF BEAM DUMPING

Beam displacement in front of absorber block TIDV	:	25 mm
Frequency	:	9.0 kHz
Deflection angle	:	1.18 mrad
Kick strength at 400 GeV/c	:	1.58 Tm
Gap width w (horizontal)	:	90.0 mm
Gap height h (vertical)	:	56.0 mm
Number of modules	:	2
Module length	:	1.2 m
Magnetic field	:	0.66 T
Current amplitude	:	30.2 kA
Inductance per module	:	2.4 μH
Voltage on magnet	:	4.1 kV
Maximum dI/dt	:	1.7 kA/μs

Fig. 2 Main parameters of the horizontally sweeping magnets (MKDH)

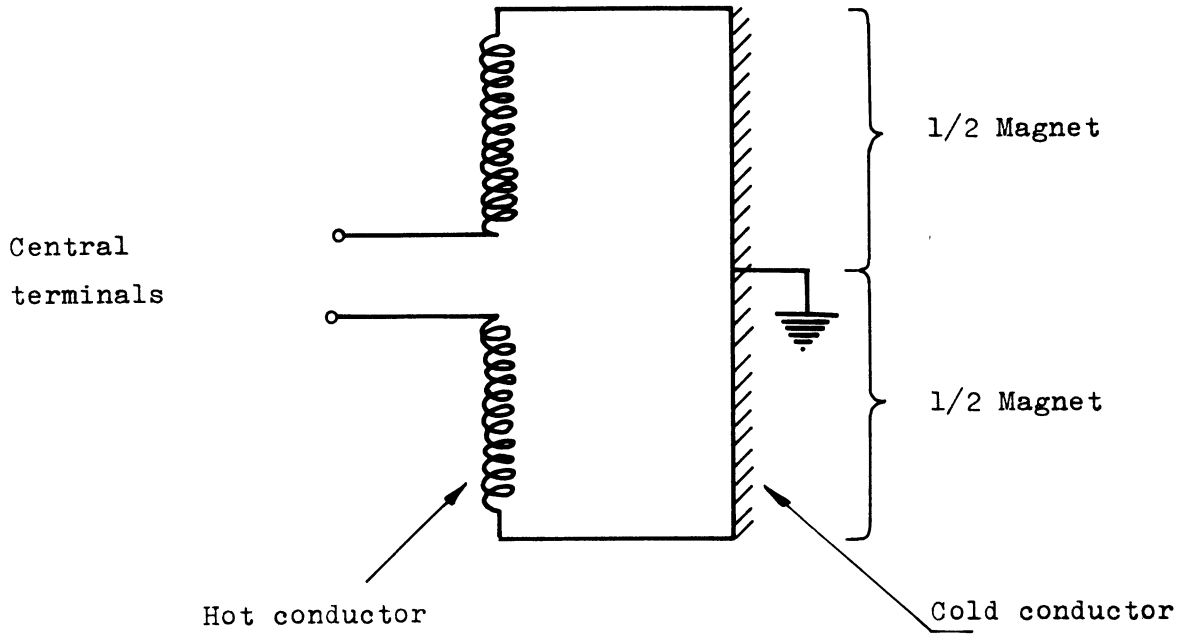

Figure 3 : Electrical circuit of the Sweeper magnet.

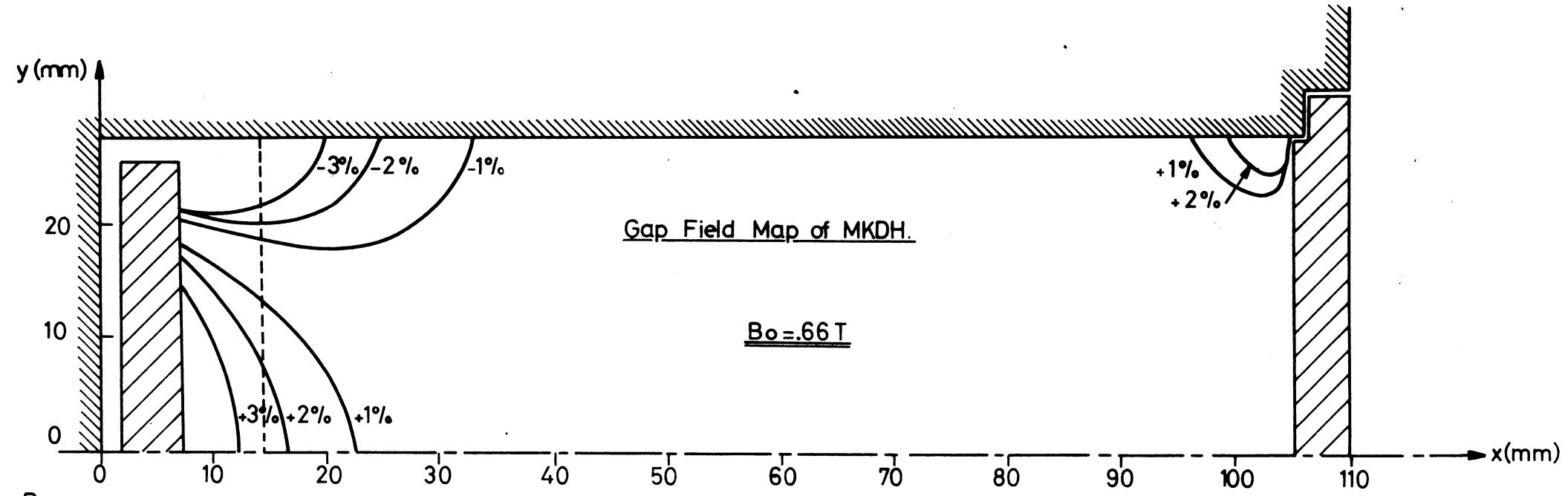

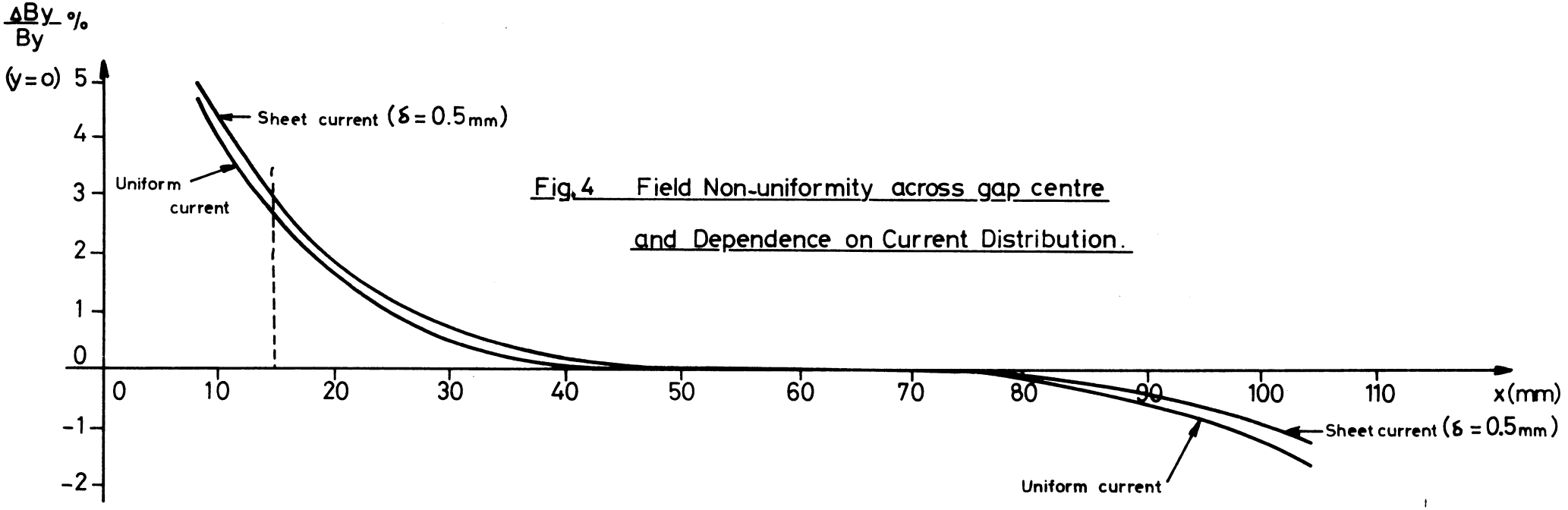

Fig. 4 Field Non-uniformity across gap centre and Dependence on Current Distribution.

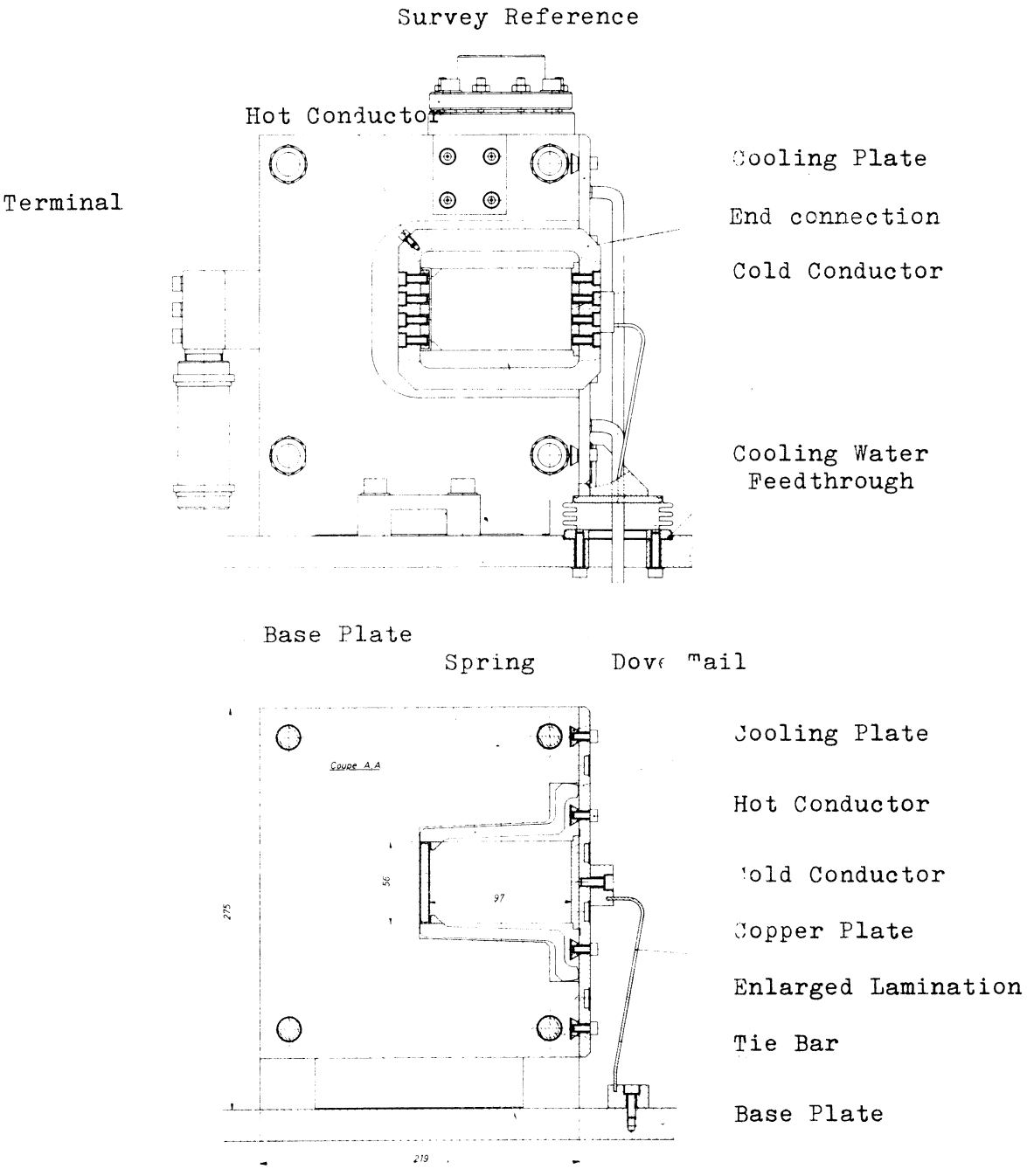

Fig. 5 Crossection of the sweeper yoke.

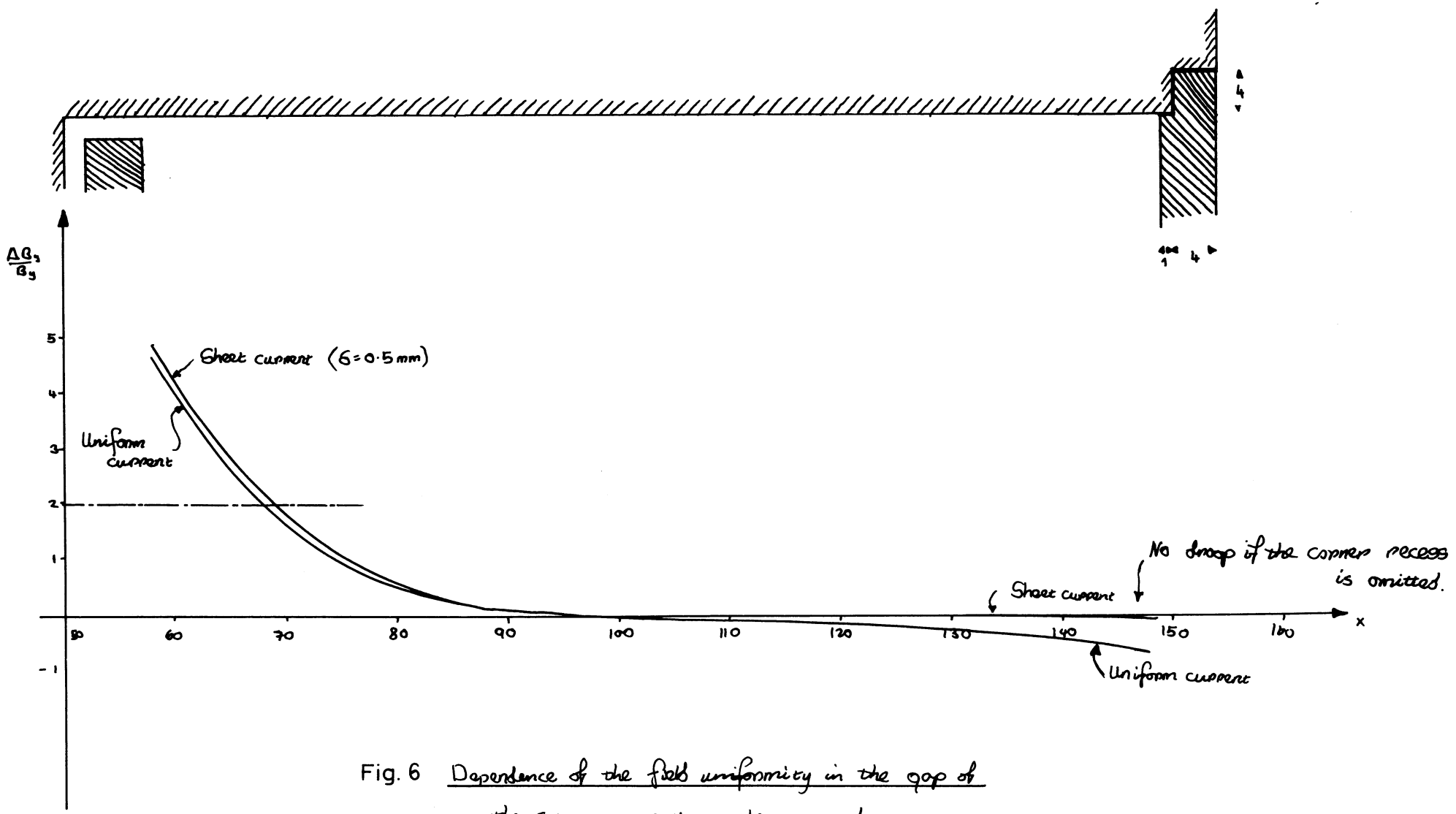

Fig. 6 Dependence of the field uniformity in the gap of the sweeper magnet on the assumed current distribution in the conductors

CGH 21/3/73

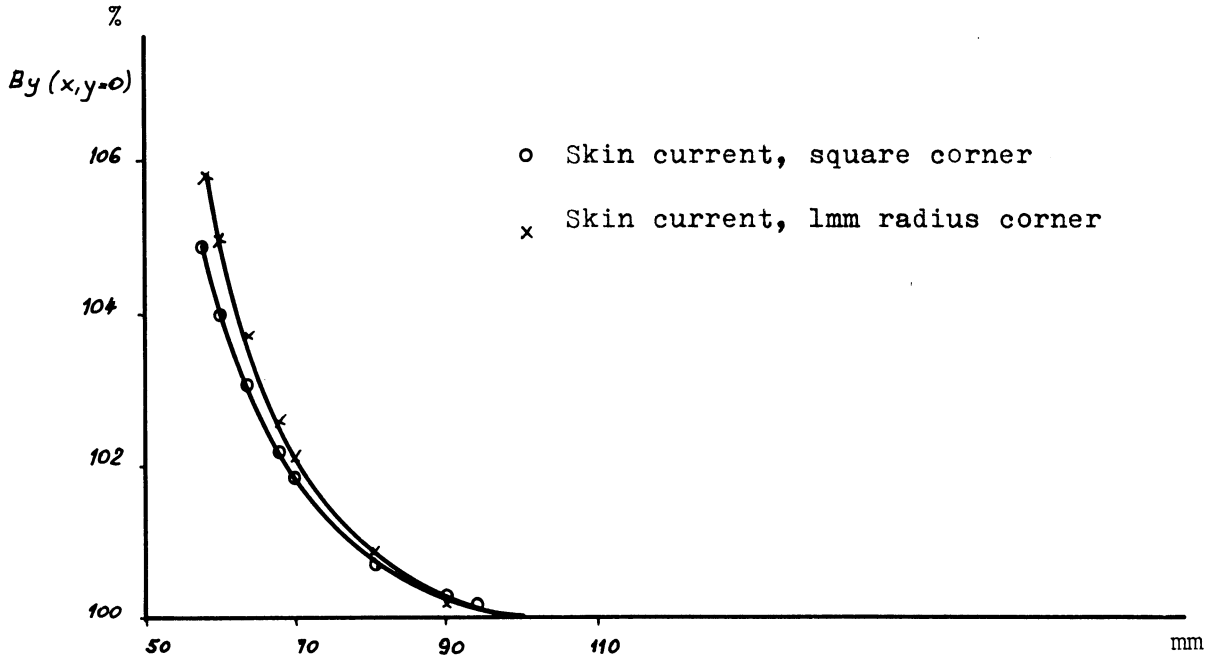

Fig.7 : Effect of corner radius on inner conductor.

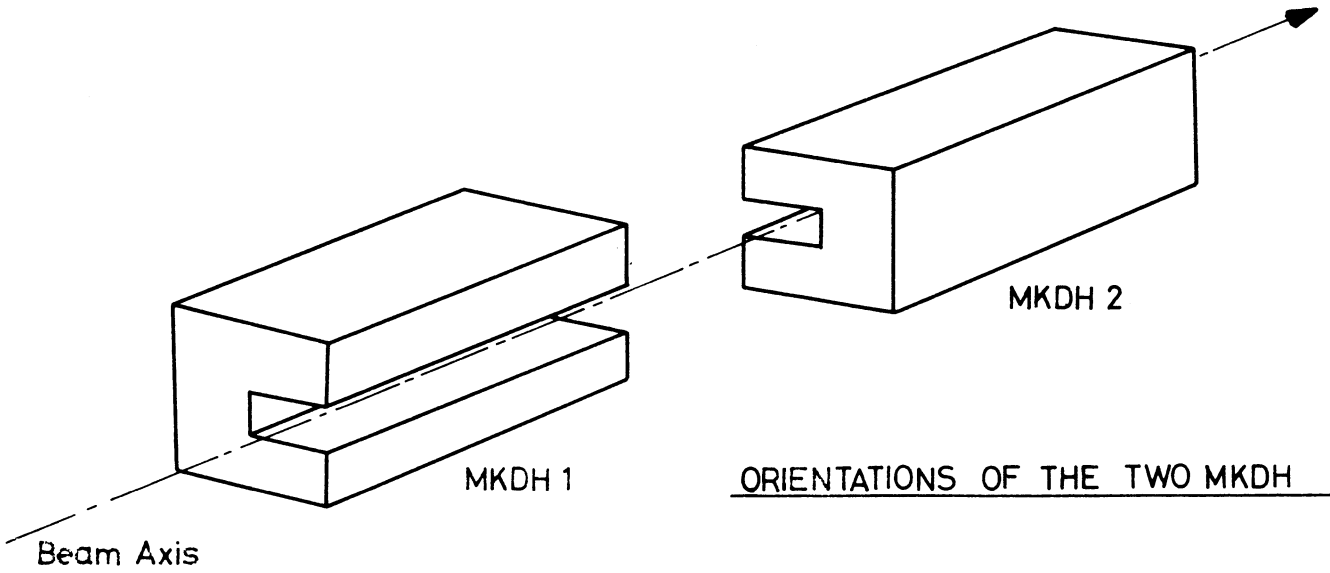

ORIENTATIONS OF THE TWO MKDH MAGNETS.

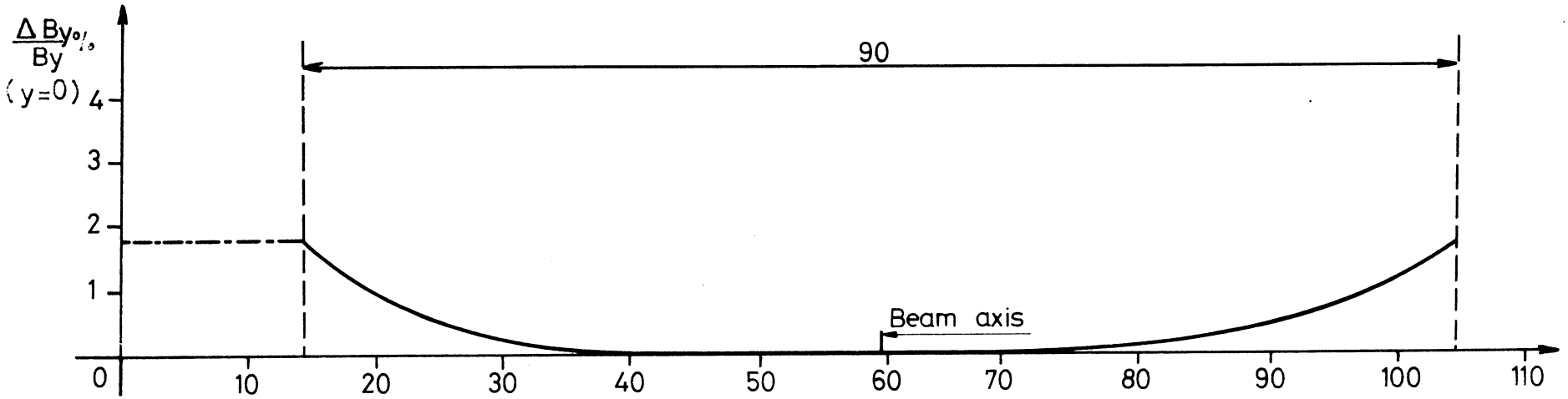

Fig. 8 NET NON-UNIFORMITY OF THE FIELD DISTRIBUTIONS OF THE TWO MKDH MAGNETS. $\left(\frac{\Delta B}{B}\right)_{max} = +1.8\%$

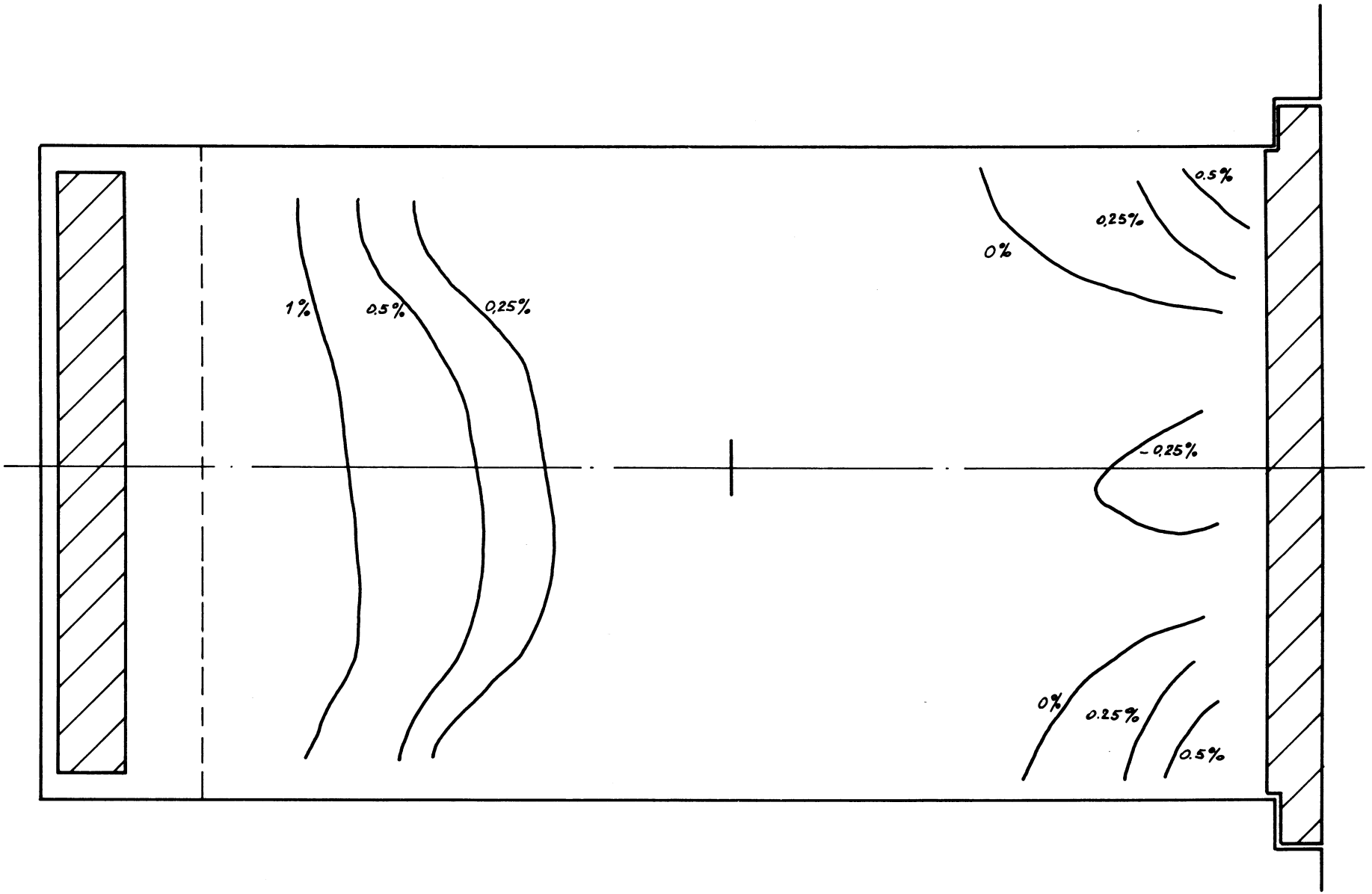

Fig.9 : Measured gap uniformity.

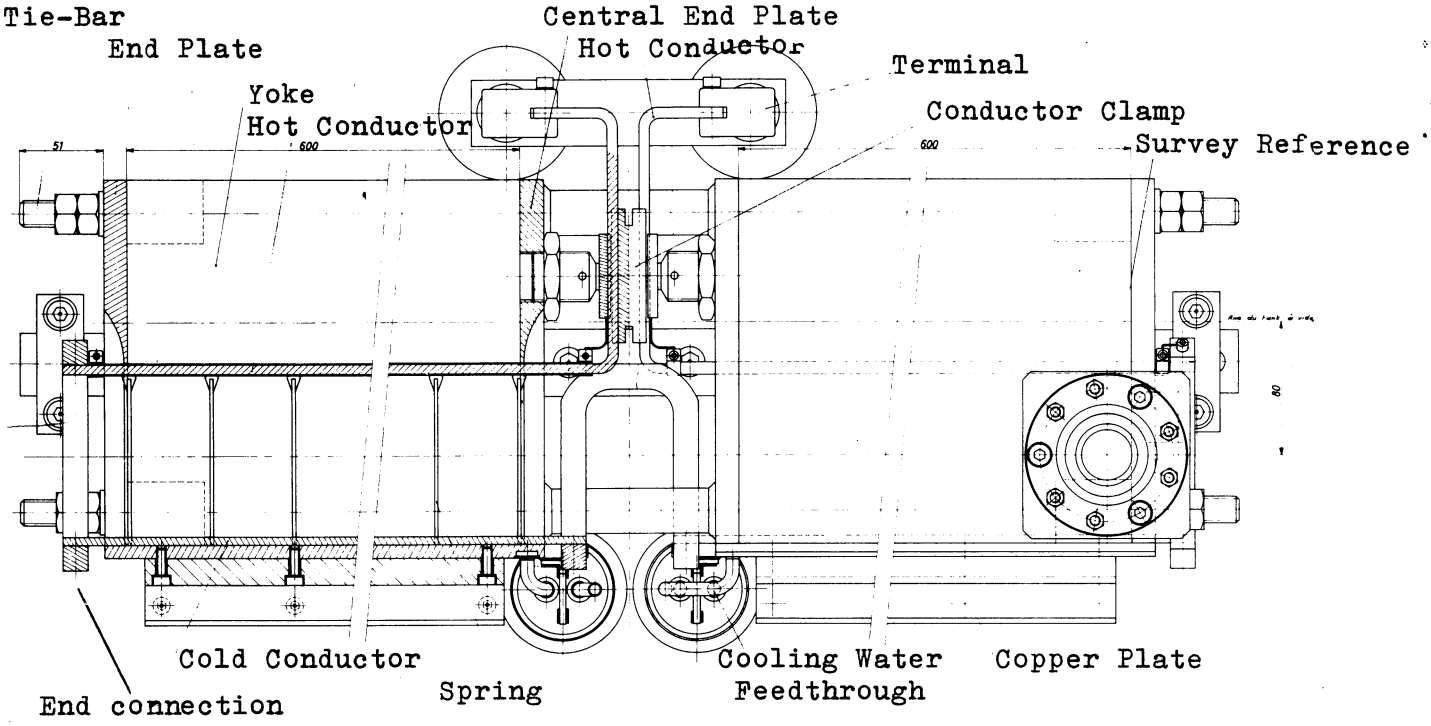

Fig.10 : Plan view of the Sweeper Magnet with end and terminal connexions.

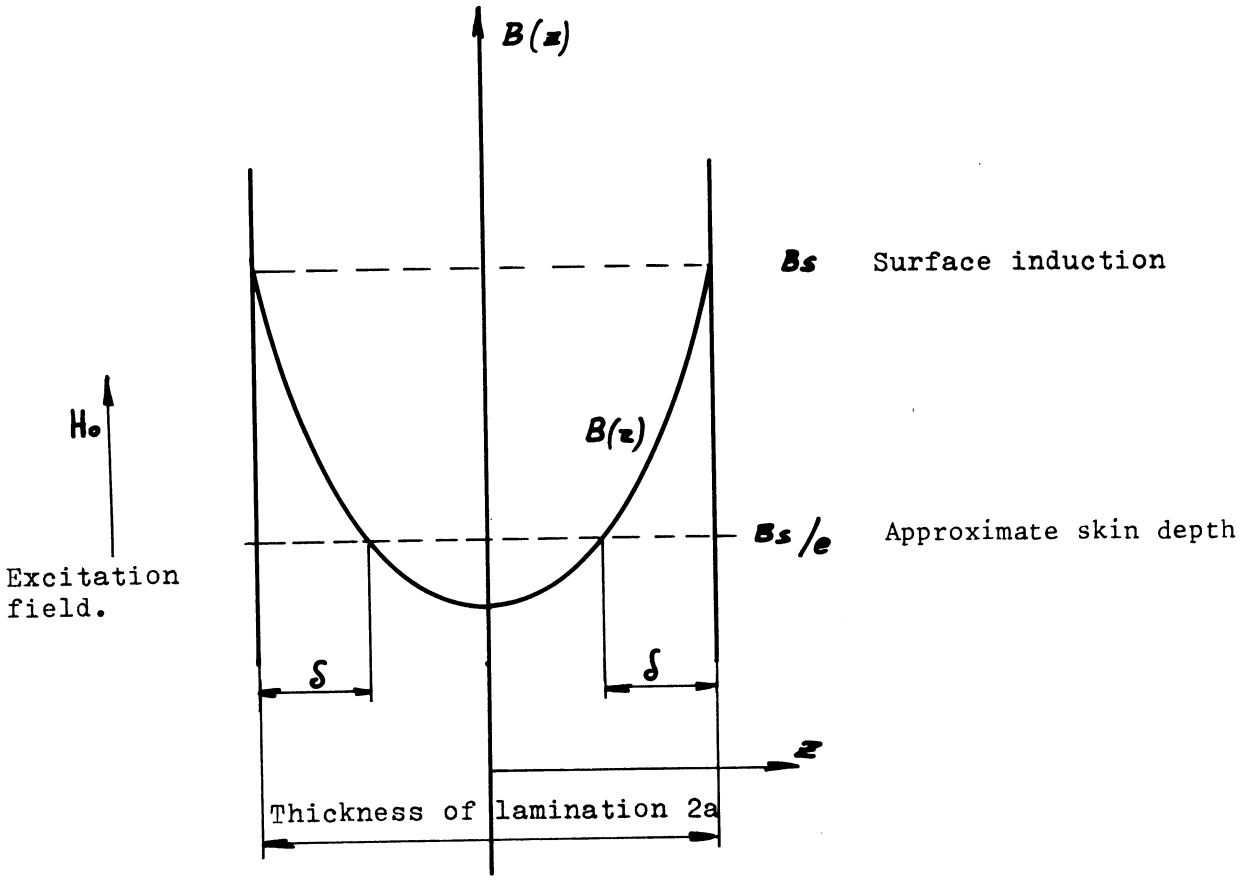

Fig.11 : Flux density distribution B (z) across a lamination produced by eddy current effects.

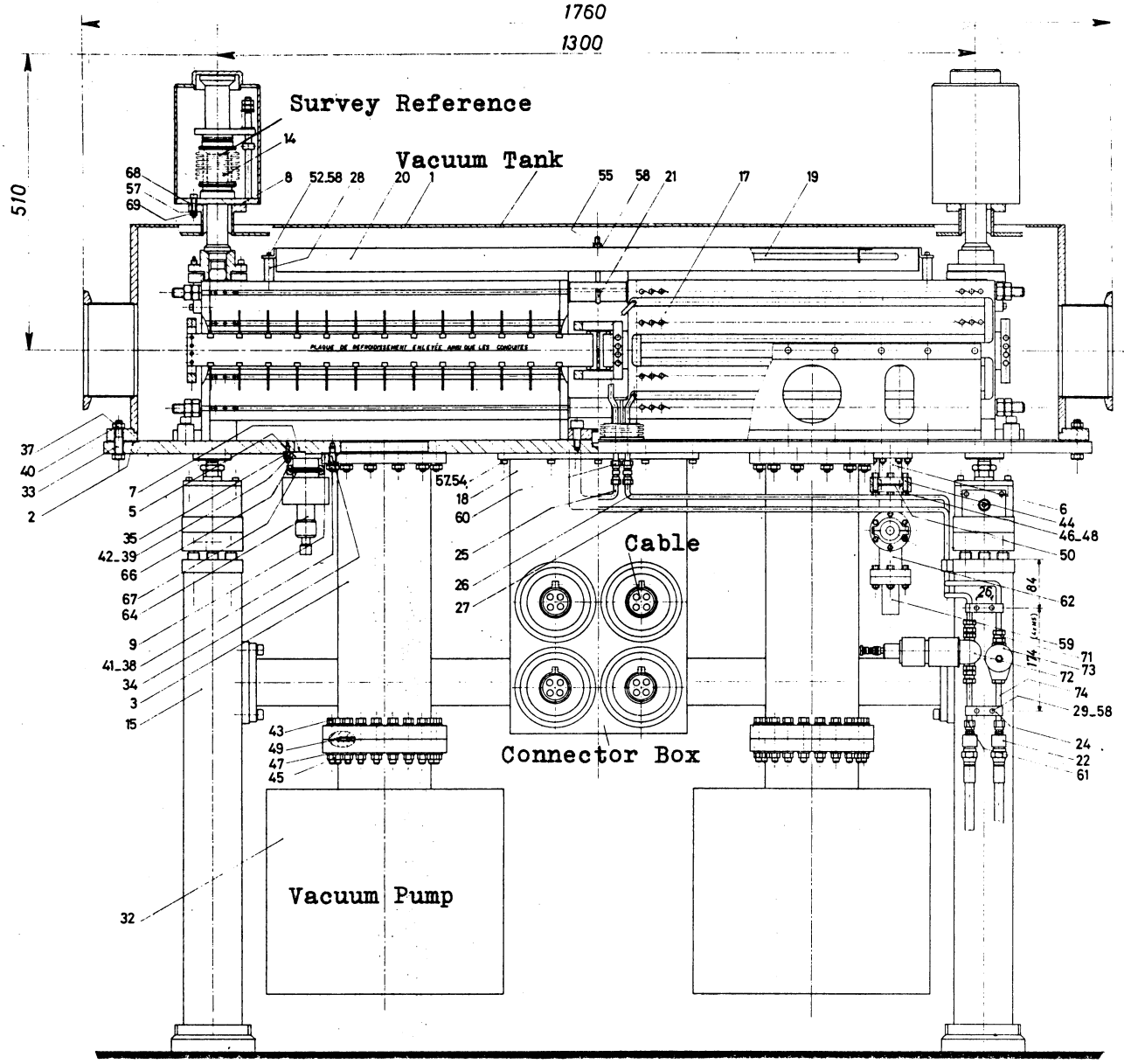

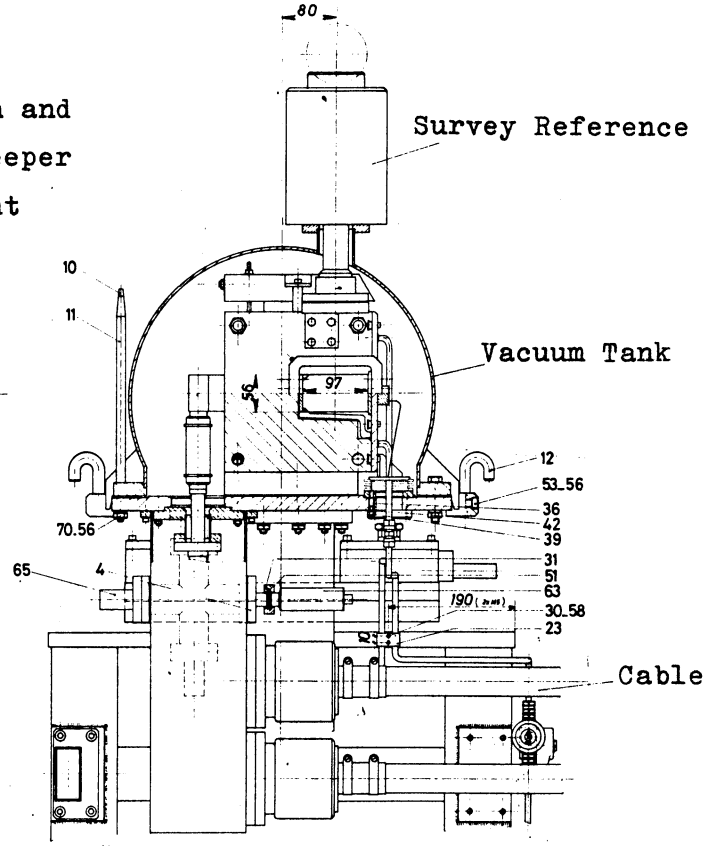

Fig.12 : Crossection and elevation of the Sweeper Magnet with one front plate removed.(left)

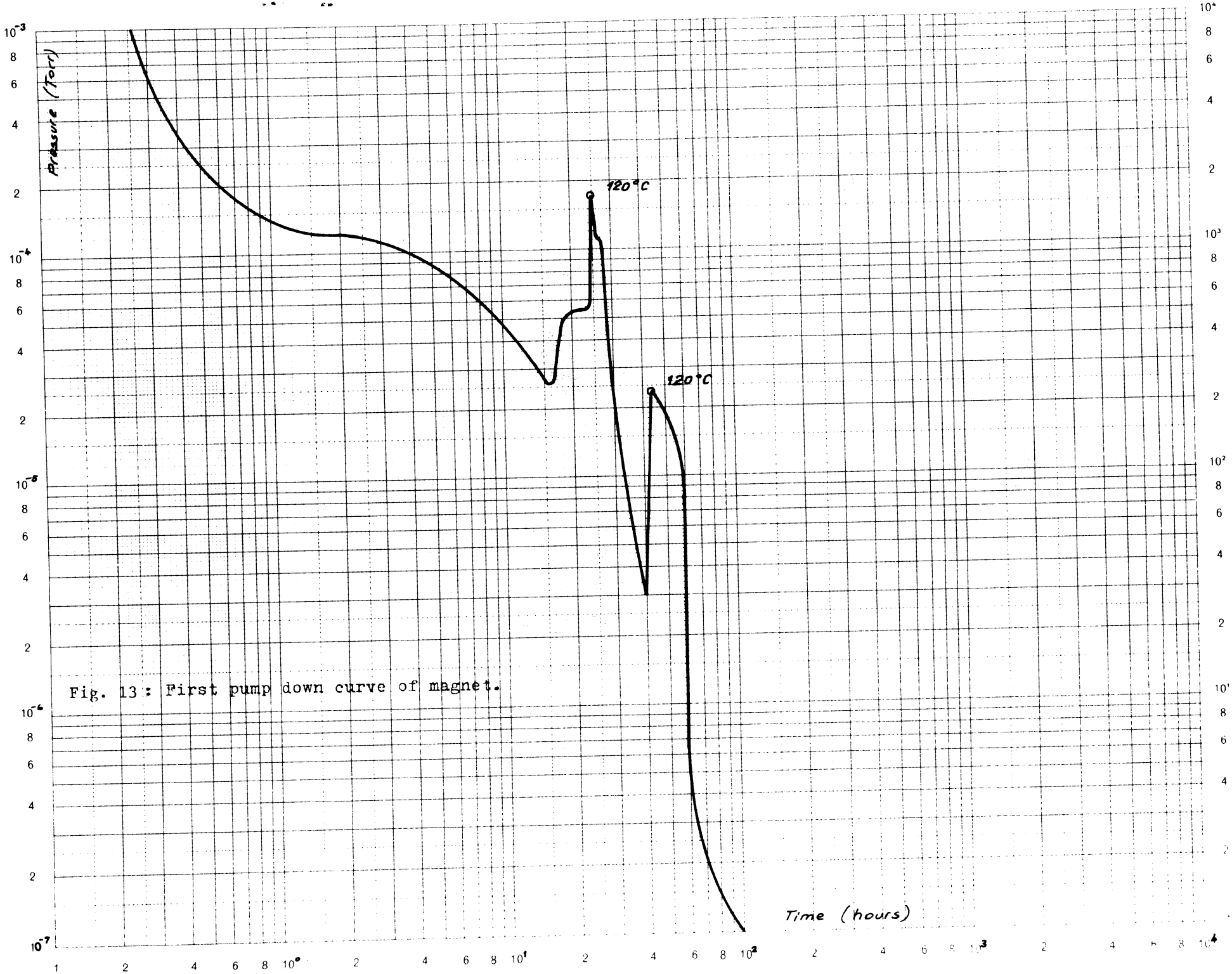

Fig. 13 : First pump down curve of magnet.

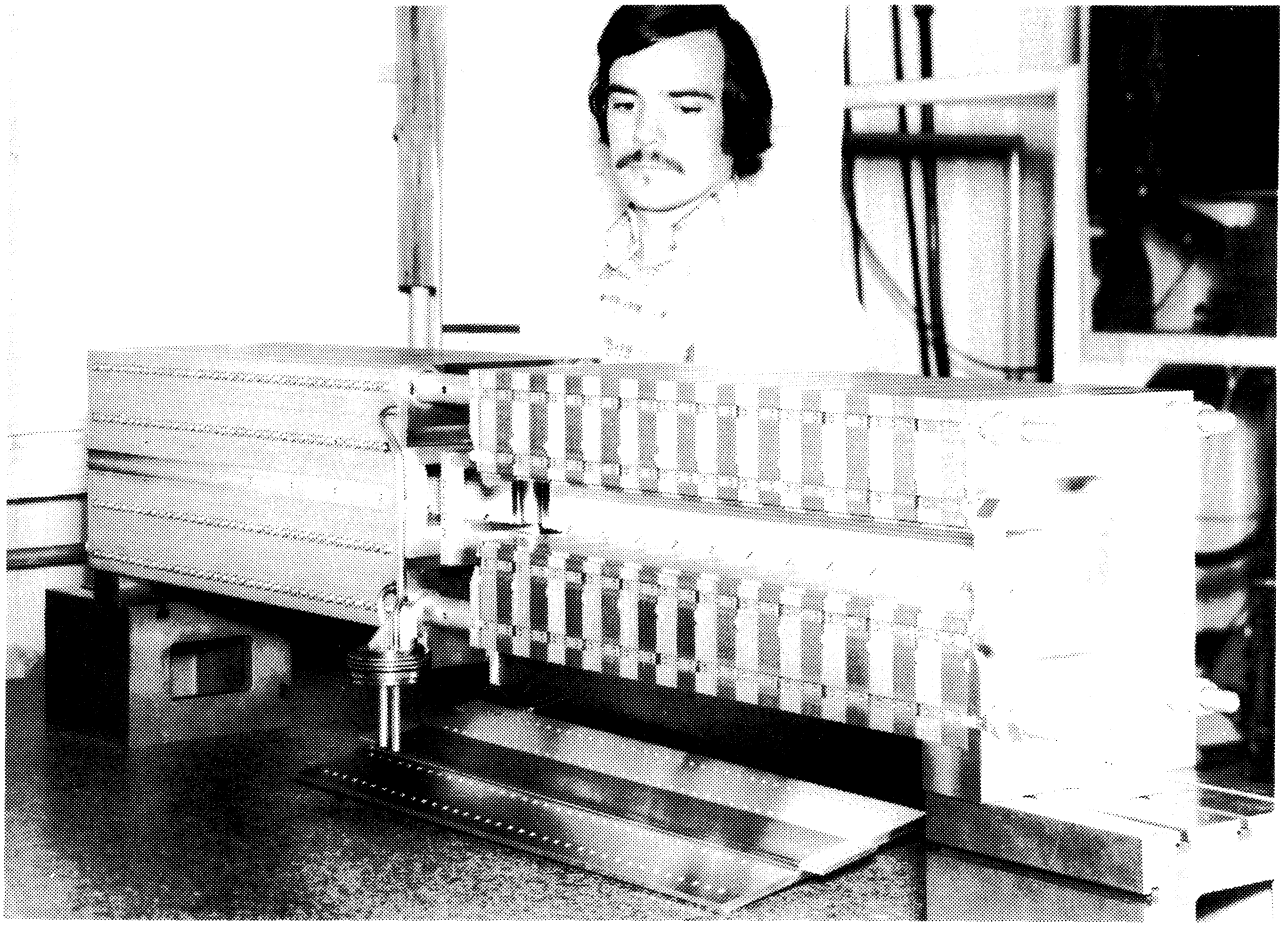

Fig.14 : Final stages of the assembly of the Sweeper magnet yoke.

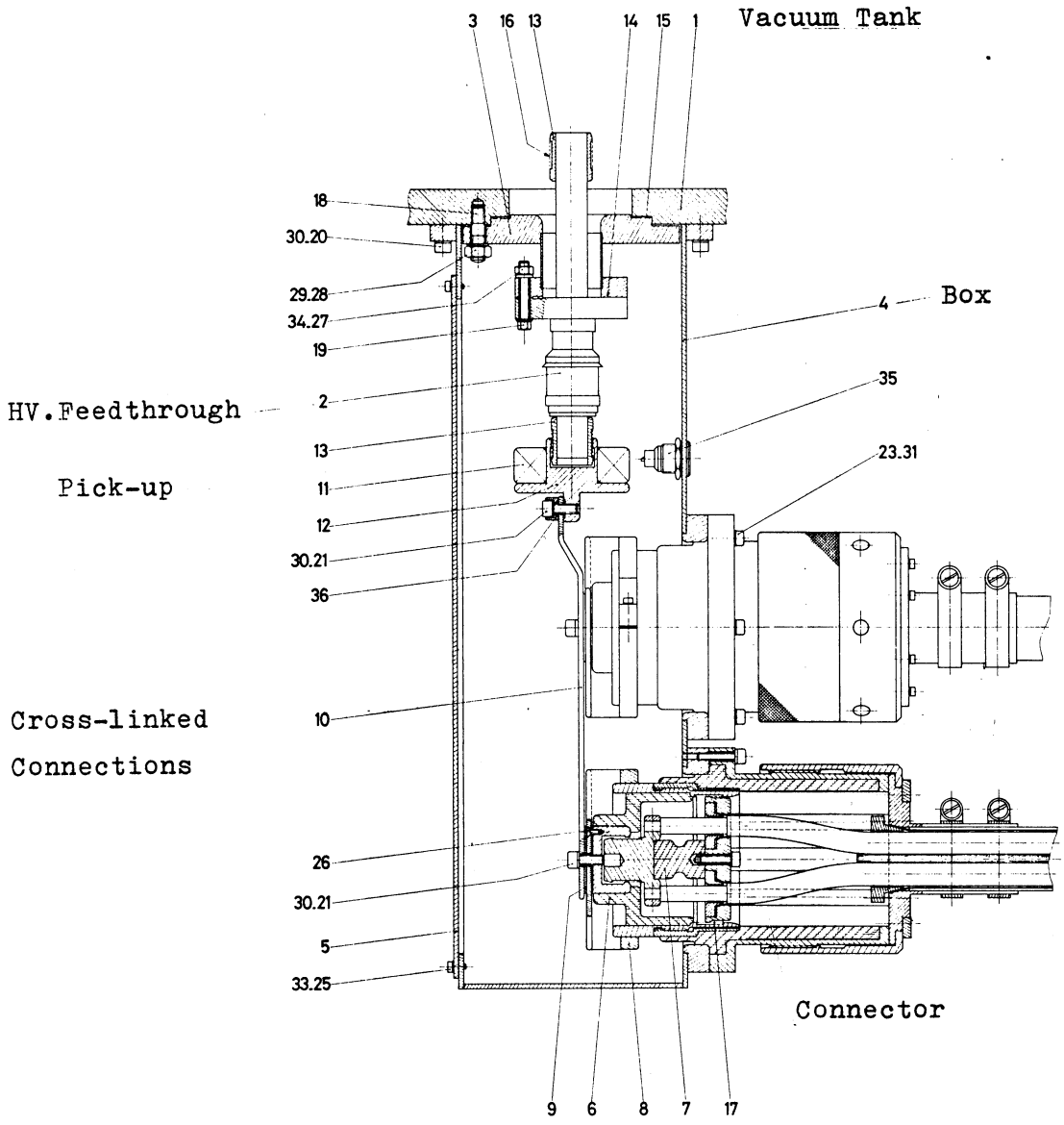

Fig.15: Connector Box with 4 cable connectors

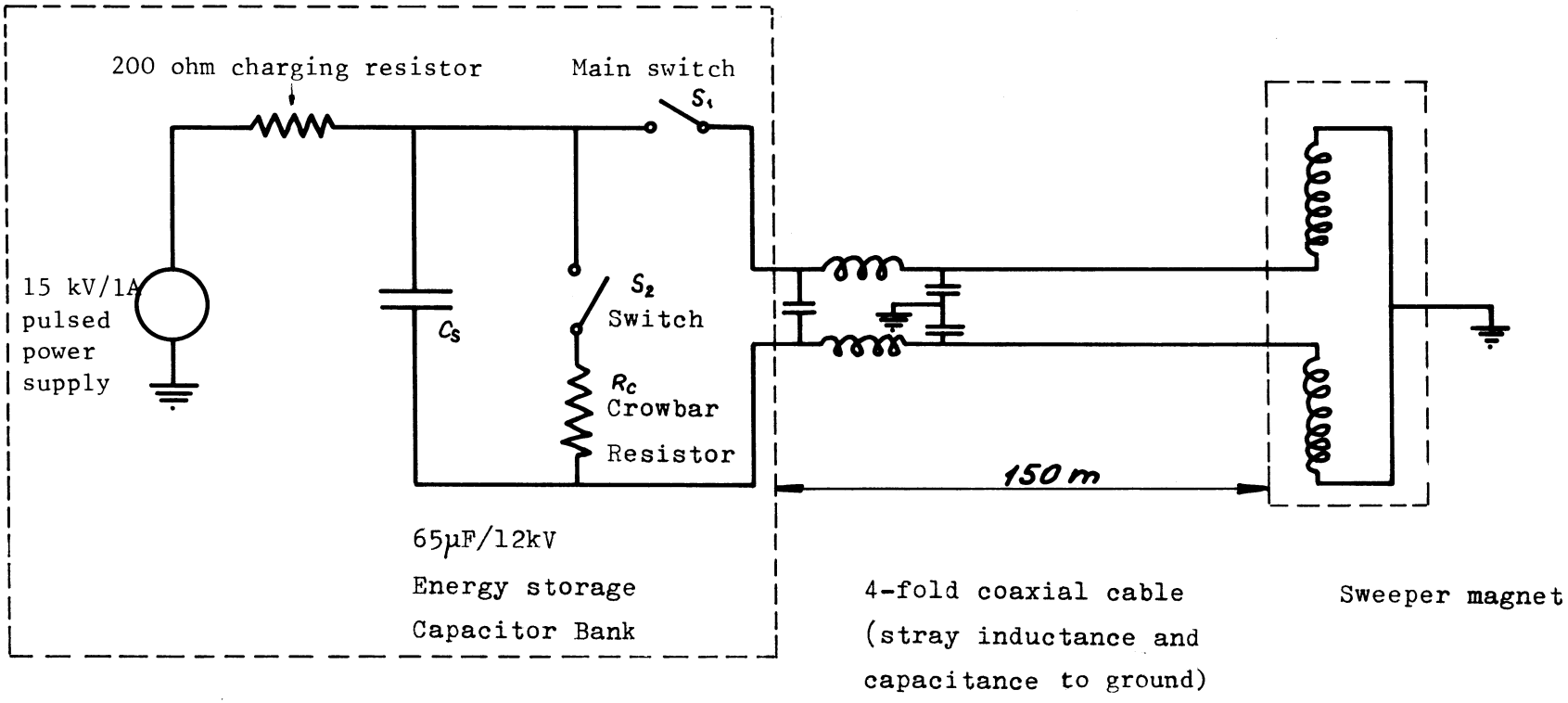

Figure 16 : Electrical circuit of the Sweeper pulse generator, transmission cable and magnet.

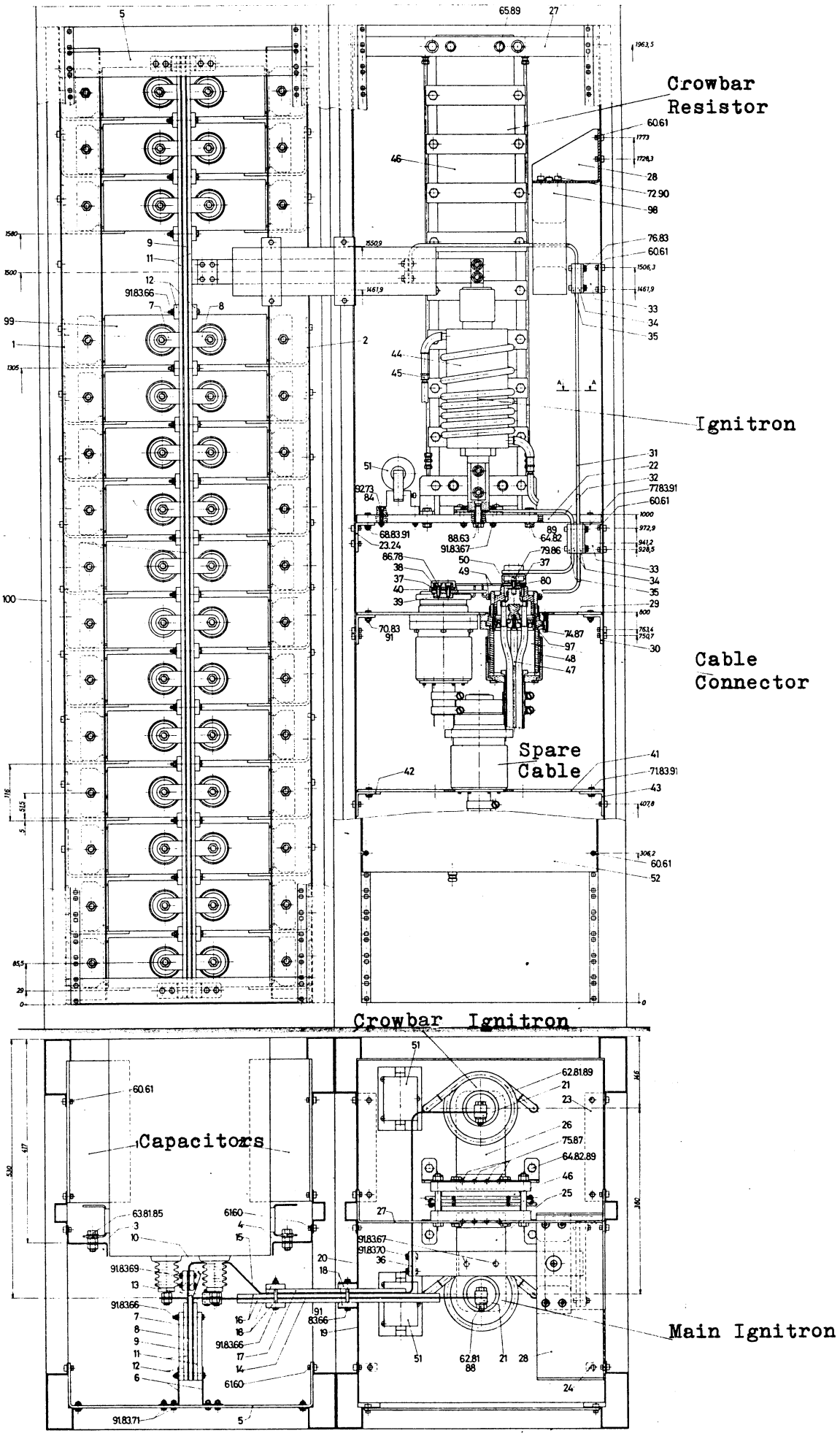

Fig.17: Section and elevation of the Sweeper Magnet pulse generator.

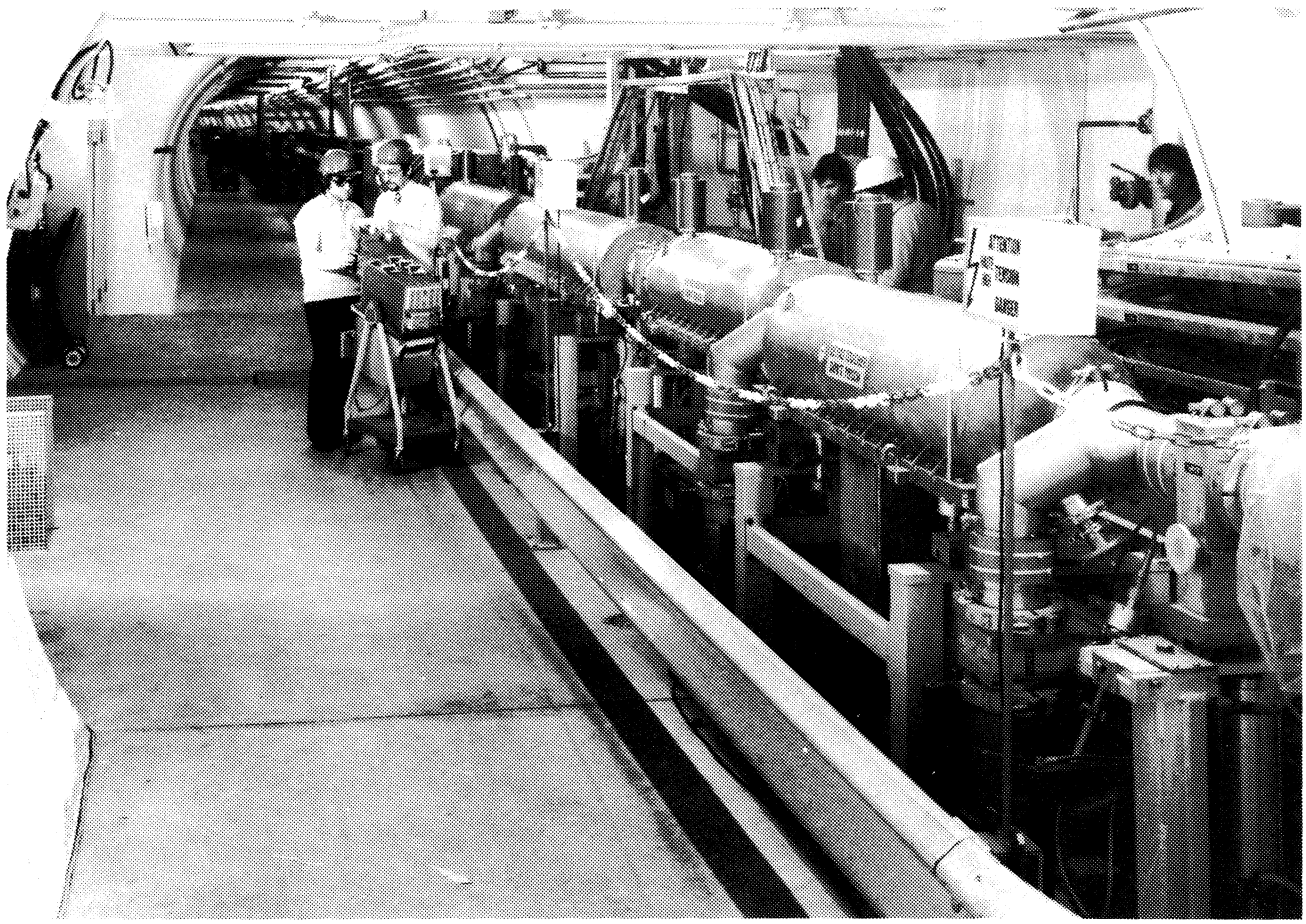

Fig. 18 : Beam dumping magnet installation in the SPS tunnel (LSS4). Foreground - the two MKDH magnets, background - the two MKDV magnets.

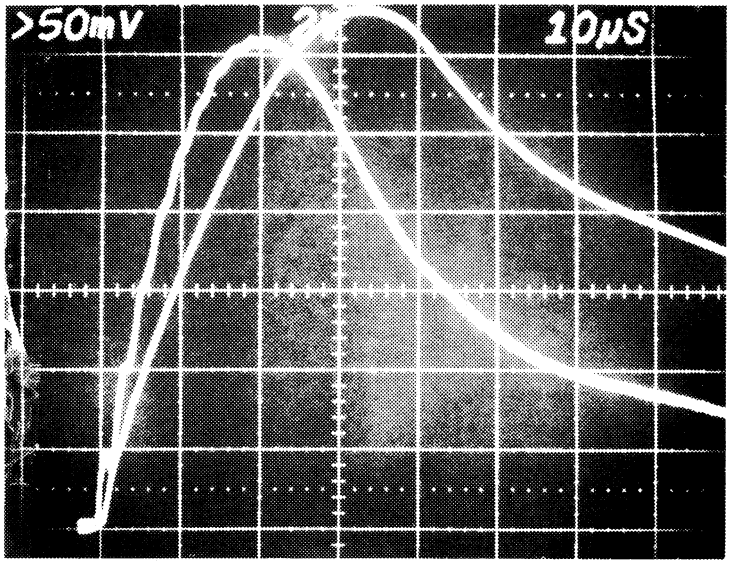

Fig. 19 The magnet current and magnet field curves at a charging voltage of 4 kV giving a peak current of 11.1 kA measured by the Pearson transformer.

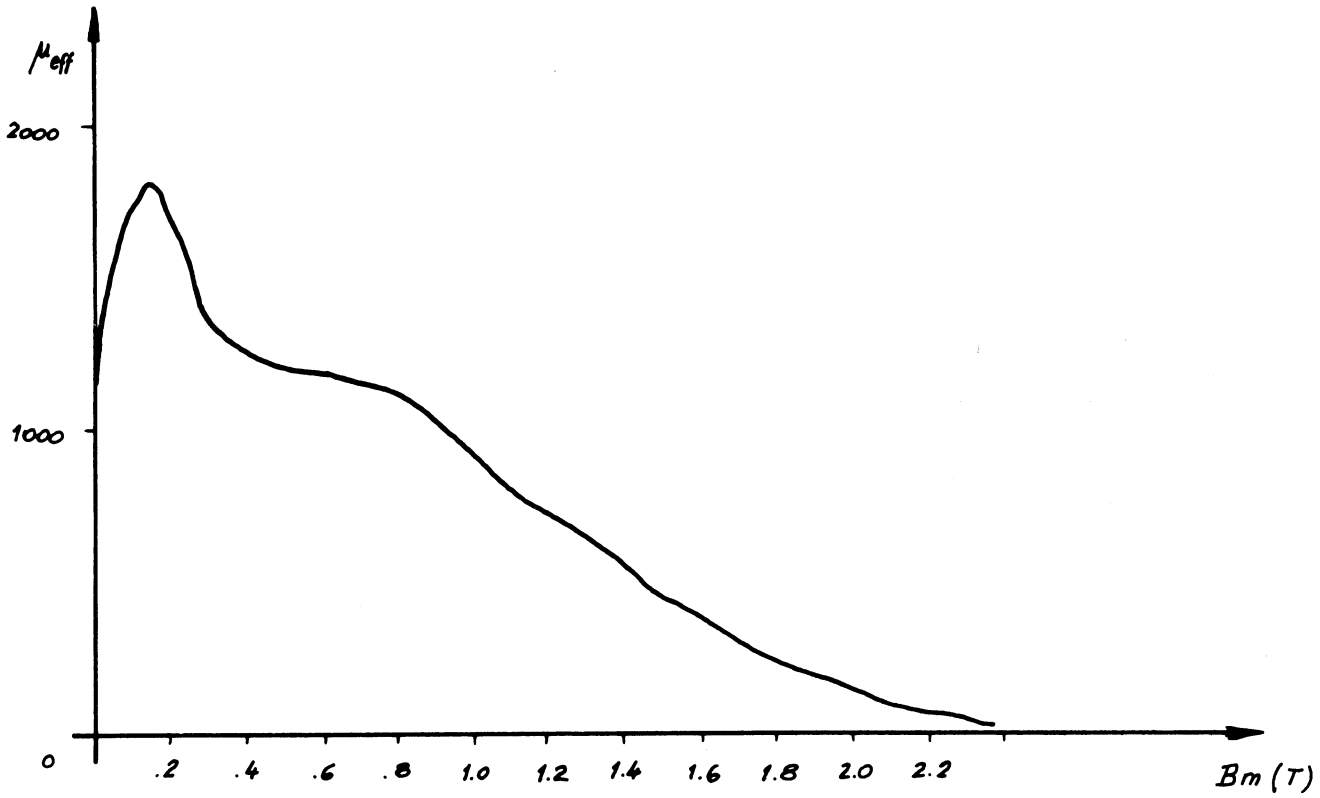

Fig. 20 : Effective Permeability of 4% silicon iron .
Pulse Frequency : 9.05 kHz
Lamination thickness : 0.3 mm